On the Structure of Superbasic (MgO)n sites solvated in a Faujasite Zeolite

PCCP

Accepted Manuscript

This article can be cited before page numbers have been issued, to do this please use: J. G. Vitillo, T. Fjermestad, M. D'Amore, M. Milanesio, L. Palin, G. Ricchiardi and S. Bordiga, *Phys. Chem. Chem. Phys.*, 2018, DOI: 10.1039/C8CP01788C.

ROYAL SOCIETY OF CHEMISTRY

rsc.li/pccp

View Article Online
DOI: 10.1039/C8CP01788C

Journal Name

ARTICLE

On the Structure of Superbasic $(MgO)_n$ sites solvated in a Faujasite Zeolite

Received 00th January 20xx,
Accepted 00th January 20xx

DOI: 10.1039/x0xx00000x

www.rsc.org/

Jenny G. Vitillo,[b]* Torstein Fjermestad[a] , Maddalena D'Amore[a] , Marco Milanesio[d], Luca Palin[c,d], Gabriele Ricchiardi[a]* and Silvia Bordiga[a]

We report the synthesis and characterisation of a HY/MgO zeolite/oxide nanocomposite material with high crystallinity and highly dispersed, highly basic MgO sites. Preparation was optimized in order to preserve sample crystallinity, to avoid the formation of mesoporosity and to minimize the formation of separate Mg-containing phases. These features were checked by means of electron microscopy, X-ray powder diffraction, porosimetry and IR spectroscopy. A highly dispersed material was obtained, comprising nanoclusters of magnesium oxide and hydroxide hosted by the microporous zeolite framework. The location and structure of the Mg-containing clusters have been studied by means of a combination of Rietveld refinement of XRPD data and high quality quantum mechanical simulations. The refinement has shown the presence of magnesium and oxygen atoms in the double six-membered ring cages, consistent with the presence of mononuclear Mg moieties. However, composition and IR spectroscopy demonstrate that other Mg species must exist, likely located in the zeolite pores. In order to propose candidate structures for these species, several hypothetic periodic models of the material were built by placing $(MgO)_n$ clusters in different locations of the zeolite structure, taking into account the material composition and other constraints imposed by the experimental observations. Periodic structures with P_1 symmetry were optimized at the B3LYP-D*/DZVP level with the CRYSTAL code and classified according to their stability. Two families of possible sites were identified: highly solvated sites $(MgO)_n$ units in narrow cavities and less coordinated clusters in the supercages. The stability of these clusters appears to be regulated by the ability of Mg^{2+} and O^{2-} ions to interact with the pore walls and by the formation of Mg-OH species as result of the reaction of Mg-O couples with remaining acidic protons. The reactivity of four representative models with CO_2 has been modeled at the B3LYP-D*/TZVP level. CO_2 forms very stable linear end-on adducts with low coordinated Mg ions in most cases. Isolated sites give rise to bridge bidentate complexes in agreement with previous spectroscopic observations. The formation of hydrogen-carbonates is observed only on specific sites, through a process having a low adsorption energy because of the high deformation of the adsorption site..

[a] Department of Chemistry and NIS Interdepartment Centre, University of Turin, Via Giuria 7, 10125 Torino, Italy. E-mail: gabriele.ricchiardi@unito.it
[b] Department of Chemistry, Chemical Theory Center, and Minnesota Supercomputing Institute, University of Minnesota, 207 Pleasant Street, Minneapolis, Minnesota 55455-0431, United States. Email: jg.vitillo@gmail.com
[c] Dipartimento di Scienze e Innovazione Tecnologica, Università del Piemonte Orientale, Viale Michel 11, Alessandria, 15121, Italy.
[d] Nova Res s.r.l., Via Dolores Bello 3, 28100, Novara, Italy.

† Electronic Supplementary Information (ESI) available: details of experimental section, FTIR study of sample preparation, additional XRPD data, structural data on the optimized computational models. See DOI: 10.1039/x0xx00000x

View Article Online
DOI: 10.1039/C8CP01788C

Journal Name

ARTICLE

Introduction

Despite the development of several new microporous material types in recent years, zeolites maintain a prominent position as adsorbents and catalysts in large scale industrial processes, due to their high stability, relatively low cost and the enormous endowment of knowledge about their chemistry accumulated over the years[1]. The largest part of this knowledge relates to acidic and metal-containing zeolites, but basic zeolites have also a sound position in catalysis[2]. More generally, basic heterogeneous catalysts play a significant role in the shift to greener industrial processes[3]. Recently, basic zeolites are increasingly proposed as robust adsorbents and catalysts in emerging fields of industrial chemistry: CO_2 capture and biorefinery. Zeolite adsorbents have been proposed for CO_2 capture from flue gases[4] and from natural gas and biogas.[5] Emerging applications in catalysis are related to the conversion of oxygen containing substrates, such as the deoxygenation of bio-oils[6], the synthesis of C_4-C_8 hydrocarbons from ethanol[7], the isomerisation of glucose to fructose[8],the dehydrogenation of ethanol[9] and direct CO_2 reduction to fuels[10, 11]. All of these processes, which add to a number of well established industrial proceses, are connected to the growing field of integration of biomass feedstocks into the chemical industry.

The structure and reactivity of acidic zeolites are nowadays very clearly defined, thanks to a wealth of experimental and theoretical investigations[12]. The structure of active sites in basic zeolites is much less understood[12,13]. The study of structure and reactivity of ion exchange sites in zeolites is mature, including alkaline and alkaline earth ions conferring basicity to zeolites. However, simple ion exchange can confer only limited and weak basicity to zeolites, while stronger basicity can be obtained only by the introduction of extra-framework basic clusters, often in the form of oxides and hydroxides[14]. "Over-exchanged" zeolites containing a larger amount of cations than those necessary to balance framework aluminum are thus a wide and diverse category of basic catalysts, whose basicity, porosity and reactivity can be tuned to match that requested by the processes cited above.

The low concentration and intrinsic disorder of the species introduced in the zeolite cavities hampers a clear identification of the active sites. Metal oxides clusters in zeolite cavities have therefore often been considered as "supported oxide catalysts", as opposed to other "single site" or "well defined" zeolite catalysts.

However, many over-exchanged zeolites have a very clear and distinct reactivity, which calls for a precise definition of their active sites. On the other hand, also in the field of acidic zeolites the role of extra-framework moieties is increasingly recognized[15], prompting for a deeper study of the properties of small oxide clusters in zeolite cavities.

Faujasites (e.g. Y and X zeolites) are the elective substrates for the preparation of basic zeolites because of their large pores, high exchange capacity, and robust structure, tuneable by chemical treatments.

Magnesium oxide is a paradigmatic basic oxide adopted as catalyst in many chemical reactions, many of them involving CO_2.[16] Over-exchange of HY zeolites with Mg salts has already been adopted for producing basic catalysts for specific reactions, and the adsorption of CO_2 has been adopted as a characterization method for their basicity[14]. Diffraction patterns of MgO-containing Y zeolites are reported in Zhang et al.[7] The authors noticed a decrease of the overall intensity of the diffraction pattern but no Rietveld analysis was carried out nor were structural consideration done on the basis of the experimental patterns.

Isolated $(MgO)_n$ clusters have been previously studied both experimentally and theoretically[17,18]. Spectra and cluster compositions observed in IR resonance-enhanced multiphonon ionization experiments on neutral $(MgO)_n$ clusters (n<15) have given indication for cubic structures[19]. Computational studies investigating neutral $(MgO)_n$ clusters without direct comparison with experiments[20,21,22,23,24,25,26] , concluded that the most stable structures for a given value of *n* are cube-like, except for $(MgO)_{3n}$ clusters for which rings and stacks of rings are preferred. More recently Kwapien at al.[27], reported a systematic theoretical study of stoichiometric $(MgO)_n$ clusters in the gas phase showing that they display an unusual structural flexibility. In the case of *n=4* the cluster retains the same cubic structure of the bulk, while more distorted cages are found for other values of *n*. Mg location in ion-exchanged zeolites has been modeled in several studies [28],[29]. Models for the structure and reactivity of and CaO and MgO clusters in zeolites have been proposed in the past, especially in connection with studies on their activity in oxidation reactions[30] and on the formation of carbonates[31].Larin et al. have described model structures of Mg_2O_x (x=1-4) clusters in different zeolites, showing their interplay with ion-exchanged Mg and their ability to form non stoichiometric clusters[31] The only experimental structural information on $(MgO)_n$ clusters in zeolites available in the literature is the dimension of the clusters in a Y zeolite (MgO 11 wt% in NaY and 12wt% in MgY),

View Article Online
DOI: 10.1039/C8CP01788C

estimated to be $2<n<10$ by ESR[32] and the coordination environment for Mg that is suggested similar to that in rock-salt MgO bulk but with a lower coordination number, as evaluated by X-ray absorption spectroscopies on Mg K-edge[33].

In this work we describe the synthesis and characterization of a superbasic over-exchanged HY zeolite containing magnesium oxide and hydroxide, and our attempts to elucidate the structure of the MgO(H) moieties by means of diffractometric and computational modelling methods.

We have synthesized an over-exchanged HY zeolite by wet impregnation followed by heat treatment in vacuum, with the aim of: a) minimizing dealumination and structural damage of the zeolite; b) maximizing the dispersion of MgO and, c) minimizing the occurrence of bulk MgO outside the pores. These conditions were achieved by careful structural control by means of IR spectroscopy, a detailed X-ray diffraction/Rietveld analysis, electron microscopy and porosimetry. Particular care has been taken to preserve the structural integrity of zeolite during synthesis, avoiding the well known dealuminating effect of fast thermal water desorption, which is in fact equivalent to a steaming treatment. The structure of the obtained basic sites has been studied by FTIR, XRPD and computational models.

In our models, we have adopted the gas-phase structures as starting geometries for the investigation of MgO clusters embedded in the Faujasite structure. The characterization results and a detailed XRD/Rietveld analysis were adopted as "boundary conditions" for the construction of high accuracy quantum mechanical models. These data show the occurrence of partial ion exchange and suggest the presence of MgO clusters in the zeolite cavities, as described below.

Given the size and complexity of the models under discussion, theoretical modelling is in itself challenging. Theoretical simulations have been used to characterize zeolites and MOFs and have helped to elucidate the mechanisms of gas adsorption[34]. Specific challenges related to this work are the high number of possible structures to investigate, the large system size, and the importance of dispersive forces in determining adsorption properties. System size required a very efficient code in order to make several large calculations feasible. To this end, we have adopted the CRYSTAL17 periodic code in its massively parallel version (MPP), specifically tailored to achieve an excellent scalability on HPC systems. Finally, the critical role of dispersion forces in the porous material has been tackled by adopting dispersion-corrected functionals. A simple and widely used method consists of adding to the semilocal or hybrid functional an atom-pairwise term of the form $f(r^{-6})$ as in the semi-empirical DFT-D family of methods of Grimme et al. [35,36,37]. These have been widely applied to both molecular complexes[38,35,39] and (in its D* form) to extended systems[40,41] where the London dispersion interactions play a major role[42,43].

Particularly, dispersion corrected DFT-D* methods have been successfully applied for adsorption of CO_2 on oxides[44] and more recently to Metal-Organics Frameworks (MOFs) resulting in good agreement with novel CCSD(T) calculations[45]. This methodology has allowed here to study the interaction of the proposed superbasic sites with CO_2 and to compare the results with those of the available probe molecule experiments.

Experimental

Materials synthesis

HY zeolite. The HY sample was obtained starting from the corresponding ammonium form (NH_4Y, Zeolyst, the Netherlands, product CBV500, average SiO_2/Al_2O_3 = 5.2, Na_2O 0.2 wt%, SA 750 m^2/g, Lot. n°: 50006N02007) by degassing the zeolite up to 400°C on a vacuum line equipped with a turbomolecular pump ($P < 10^{-4}$ mbar). This thermal treatment was optimized to avoid dealumination and the formation of mesopores. The optimized temperature program is a slow ramp as follows: for a 2 g batch, 15 h at RT, 9 h at 80°C, 15 h at 150°C, 6 h at 200°C, 15 h at 250°C, 6 h at 300°C, 15 h at 350°C, 8 h at 400°C. The sample was then slowly cooled to RT under degassing and quickly transferred to a dry glove box. The use of the dry HY form of the zeolite as starting material ensures control of the stoichiometry of the successive impregnation.

MgOHY ($MgO/Mg(OH)_2$/HY composite). For each batch, 0.5 g of dehydrated HY were immersed in 5 ml of an aqueous solution of $Mg(NO_3)_2 \cdot 6\ H_2O$ (Sigma Aldrich, $Mg(NO_3)_2 \cdot 6\ H_2O$ to HY weight ratio of 0.53 corresponding to a final MgO to HY weight ratio of 0.084, or 7.76 wt.%). This corresponds to an excess in Mg^{2+} ions with respect to the H^+ ions present in the zeolite ($Mg^{2+}/2H^+$ = 1.36). The solution was stirred for 30 min at RT and then it was transferred to a rotary evaporator in order to dry it at 25°C. The dry powder was then degassed up to 400°C to obtain MgOHY by using the same slow thermal program adopted for HY. Because of the well-known reactivity of MgO clusters with atmospheric CO_2 also at RT, after the synthesis, the materials have been handled in inert atmosphere in order to avoid hydration and carbonation reactions (M Braun Lab Star Glove Box supplied with pure 5.5 grade Nitrogen, O_2<0.5 ppm, H_2O <0.5 ppm).

MgO. An unsupported MgO reference sample was obtained by treating $Mg(NO_3)_2 \cdot 6\ H_2O$ following the same procedure used for MgOHY. The material was stored in a glove box, avoiding the contact with air.

Instrumentation

Nitrogen volumetry. Nitrogen adsorption isotherms were measured on a commercial volumetric apparatus (Micromeritics ASAP2020) at 77 K. Before measurement, the powders were degassed at 400°C on a vacuum line equipped with a turbomolecular pump and then the samples were transferred in the measurement cell in a glove box. The specific surface area was obtained by using the Langmuir[46, 47] approximation in the standard pressure range ($0.05 < p/p_0 < 0.20$). Pore size distribution was evaluated using the Non-Local DFT (Density Functional Theory) method on the basis of the cylindrical pore model proposed by Tarazona[48] and the cylindrical pores/oxide model as implemented in the Micromeritics software. The qualitative description provided by the two models on the changes of HY porosity after the

View Article Online
DOI: 10.1039/C8CP01788C

introduction of MgO species was identical. Being the Tarazona model underestimating the dimension of the zeolite pore of about 4 Å with respect to the crystallographic value, only the results obtained with the oxide model were reporting in the following. The micropore volume and the surface area external to the micropores (S_{ext}) have been evaluated with the t-plot method adopting the Harkins and Jura equation of thickness in the $0.15 < p/p_0 < 0.50$ range.[46] All the reported quantities are affected by an error of approximately 10%.

XRPD. X-Ray Powder Diffraction measurements were performed in the 2θ range 2° – 100° (step size of 0.0167°, time per step 850 s) in Debye-Scherrer geometry using a laboratory diffractometer (Panalytical X'Pert Pro Multipurpose Diffractometer) having as source a high power ceramic tube PW3373/10 LFF with a Cu anode equipped with a Ni filter to attenuate K_β and focused by a PW3152/63 X-ray mirror. The incident beam was collimated by a Soller slit (0.04 rad), an antiscatter slit (1/2 Å) and a divergence slit (1/2 Å); for the diffracted beam an antiscatter slit (AS Slit 5.0 mm, X'Celerator) and a Soller slit (0.04 rad) were adopted. Samples were sealed into boron silica glass capillaries of internal diameter 0.8 mm in a protected atmosphere and mounted on a rotating goniometer head.

The Rietveld analysis has been performed by using the program Topas TA.[49] Real space search for MgO moieties was performed by simulated annealing procedure as implemented in Topas TA. Crystal and molecular drawings were carried out by Mercury and VESTA [50, 51] The two refined structures of the Y zeolite without and with MgO were deposited within the COD database with entry numbers 3000174 and 3000175.

TEM Microscopy. Transmission Electron Microscopy analysis was obtained using a JEOL 3010-UHR instrument operating at 300 kV, equipped with a (2k × 2k) pixels Gatan US1000 CCD camera and with an OXFORD INCA EDS instrument for atomic recognition via energy dispersive spectroscopy (EDS) on the Kα of the elements considered. The powdered samples were deposited on a lacey carbon film covered 200 mesh copper grids (Structure Probe, Inc.).

FTIR spectroscopy in static gas conditions. In situ FTIR spectra in transmission mode (2 cm^{-1} resolution, average on 32 scans) were collected on a Bruker Vertex70 spectrophotometer. The samples were measured in the form of self-supporting pellets inside a quartz cell in controlled atmosphere.

Computational Models

Given the composition of the HY zeolite described above (Si/Al ratio =2.6), models of the pure HY host structure were built with 13 Al atoms distributed over the 48 available T sites of the unit cell ($H_{13}O_{96}Al_{13}Si_{35}$, Si/Al= 2.692) of the unit cell. Models were constructed by randomly placing the Al atoms on T sites, respecting Löwenstein's rule[52]. Protons were placed randomly, subject to the following two constraints: 1) only 1 proton per Al tetrahedron, 2) no proton on O(4), thus respecting the experimental findings of Czjzek et al.[53] We adopted the following proton distribution (atom numbering as in Ref. [53]): 7 protons on O(1), 2 protons on O(2), and 4 protons on O(3). P1 symmetry was adopted, and cell parameters were fully optimized. MgO models were constructed in order to comply with the experimental MgO content of 8.2±1 wt% (see below), corresponding to the presence of about 4 formula units of MgO per unit cell of zeolite HY. Two types of models were built: *isolated MgO units* and $(MgO)_n$ *cluster* models. In isolated models, four MgO molecules were placed in in the zeolite. *Cluster* models comprised a variety of $(MgO)_n$ clusters. All types of clusters were placed initially both in different locations of the supercage and in the sodalite cage, in order to explore the solvating properties of cavities with different size. Given the high gas phase stability of the $(MgO)_4$ clusters and the fact that the introduction of 1 such cluster per zeolite unit cell corresponds approximately to the experimental MgO loading of the composite, $(MgO)_4$ clusters were studied systematically in great detail. $(MgO)_4$ moieties were placed at different starting locations, exploring the proximity of the MgO/Mg_4O_4 units with different rings (4- and 6-membered) with a different number of Al atoms per ring (0-3). In addition to $(MgO)_4$ clusters, the following other models were evaluated: a) $(MgO)_n$ clusters with n=3 and 7; b) $Mg_4(OH)_8$ cubic hydroxide clusters. A total of 30 structures were optimized and compared. In the following, only the results obtained for isolated and $(MgO)_4$ clusters will be described, for reasons discussed in the next section. Since the models were constructed by adding basic MgO to the acidic HY zeolite, they lead to the formation of OH groups and water, and this acid-base reaction strongly affects the energetics of the system.

All calculations were performed with the CRYSTAL17 package, a periodic *ab-initio* code based on atom centered Gaussian basis sets[54]. Notably, the use of an atom-centered basis set in this code permits the accurate and easy evaluation of the exact HF exchange, so that it can efficiently deal with hybrid functionals for periodic systems. Geometry optimization were performed using the hybrid B3LYP functional of widespread use in materials science. It includes part of the exact Hartree-Fock exchange, which reduces the self-interaction error and improves the performance in the description of structure of solids[55]. Dispersion interactions were modeled with an empirical correction, where the total computed energy is given by Equation

$$E_{(DFT-D)} = E_{DFT} + E_{disp}$$

where E_{disp} is the empirical D2 dispersion correction originally proposed by Grimme in its reparametrization for crystals (B3LYP-D*) [40]:

$$E_{disp} = S_6 \sum_g \sum_{ij} f\left(R_{ij,g}\right) \frac{C_6^{ij}}{R_{ij,g}^6}$$

With reference to CRYSTAL17 user's manual, in the evaluation of the Coulomb and Hartree-Fock exchange series, the five threshold parameters (determining the level of accuracy) were set at 7 7 7 7 18 values. The threshold on the SCF energy was set to 10^{-8} Ha for the geometry optimization and the reciprocal space was sampled according to a regular sublattice with shrinking factor equal to 1. A first screening of possible structures including the above mentioned clusters of MgO at different chemically reasonable sites of zeolite was performed by using an already well performing basis set of double-ζ plus

View Article Online
DOI: 10.1039/C8CP01788C

polarization quality (hereafter DZVP) comprising: the Nada 88-31G*[56] on Si atoms, 8-511 G* on Al atoms[57], 8-511d1G on Mg atoms[58], 8-411d1 on O atoms[59], 5-11G* on H atoms.[60] The adsorption of CO_2 molecules on selected low energy MgOHY models (see Discussion) has been simulated. Different basis sets have been adopted to describe CO_2. At first a basis of the type double-ζ plus polarization quality has also been used on the adsorbed molecule (6-31d1G Gatti 1994 for C [61] and the same basis set adopted for the oxygen of the zeolite HY for O). To better describe the interaction of CO_2 with MgO, the basis set on the adsorbate atoms has been improved to a larger basis set of triple-ζ plus polarization quality[42]: However the adoption of a mixed basis originated some misleading conclusions due to a large basis set super position error. Hence for all the atoms in proximity of the adsorption site a basis set of triple-ζ plus polarization quality was adopted: in particular, the more extended basis sets of Civalleri et al.[42] have been adopted on CO_2, and those of Ugliengo et al.[62] on the MgO clusters and on all oxygen atoms of the host zeolite bound to Mg.

Results and discussion

FTIR spectroscopy. The spectra of the HY zeolite before (black curve) and after the impregnation with $Mg(NO_3)_2 \cdot 6\ H_2O$ (dark blue curve) are reported in Figure S1 of the ESI. The latter shows the presence of two additional broad bands at 3600 cm^{-1} and at 1387 cm^{-1} associated to –OH and $–NO_3$ groups, respectively testifying the presence of the salt. The nitrate band is shifted of more than 60 cm^{-1} with respect to the position in the bulk magnesium nitrate spectrum at the same temperature (blue curve in Figure S2 in the ESI). The decomposition of the magnesium nitrate to magnesium oxide was then monitored by recording *ex situ* spectra at the increasing temperature steps considered in the synthesis for both the supported and unsupported nitrate. The collected spectra (reported in Fig S1 and S2 of the ESI) show that nitrate decomposition is complete at 400°C in both cases, although the decomposition of the supported material starts already at 200°C, whereas the spectra of the unsupported nitrate are essentially unchanged in the 95-300°C range. The larger instability of these species after supporting them on the zeolite can be associated to their larger dispersion and smaller particle dimension with respect to bulk nitrate.

Infrared spectroscopy can also provide information on the Mg-O species present in MgOHY. Fig. 1 shows the spectra recorded in transmission for HY and MgOHY, as activated at 400 °C in vacuum. Contrary to ATR, the specimen thickness sampled by the incident light is larger in transmission mode. For this reason, the changes of most intense modes of the zeolite and of the nitrate cannot be characterized as done by ATR-IR because of the saturation of the detector. On the other hand, this allows to have a very high signal to noise ratio in the region corresponding to the stretching mode of hydroxy species (3800-3200 cm^{-1}).

The spectrum of HY shows the typical pattern of OH groups with the external silanols at 3740 cm^{-1} and a family of OH acidic framework OH groups in the range 3530-3625 cm^{-1}. Upon formation of the composite, the external hydroxyls are unaffected, while the signals of the acidic -OH groups are decreased and shifted to higher wavenumbers. The presence of remaining acidic groups proves that ion exchange with Mg^{2+} takes place only on a fraction of the available sites, while the shifts observed indicate a change in the local environment of the remaining -OH groups. Moreover, two additional signals at 3690 cm^{-1} and 3676 cm^{-1} form on MgOHY.

These signals have been previously associated to small clusters of MgO hosted in the zeolite supercages, generating basic Mg^{2+}-OH^- hydroxy group[14, 63] by the reaction:

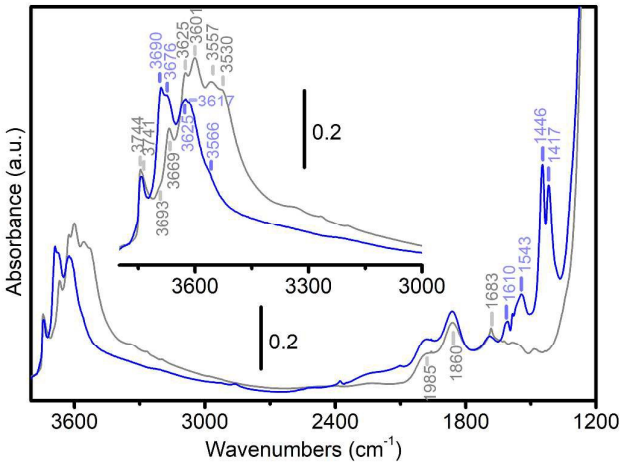

Fig. 1. FTIR spectra of HY (grey) and MgOHY (blue) after activation at 400°C in vacuum overnight. In the inset, the region of the spectra corresponding to that typical of hydroxy stretching modes.

$$Mg^{2+} + H_2O \rightarrow Mg(OH)^+ + H^+$$

The size of the clusters was estimated between 2 and 10 metal-oxygen units[32] and they were observed to form also by migration of Mg ions from their exchange sites upon thermal treatment. In the spectra of MgOHY, the presence of two additional bands at 1446 and 1417 cm-1 is evident. Such doublets have been previously associated to nitrate or carbonate species in Y zeolites. Although the assignment of these bands to nitrate species would be straighforward, EDS analysis did not evidence the residual presence of N, using both EDS-TEM and EDS-SEM (see Figure S3c'). Moreover, the pure nitrate sample was completely decomposed at this temperature (see Figure S2) and the thermal stability of these species after dispersion is expected to be lower. These bands are likely due to the formation of carbonate and bicarbonate-like species due to contamination of the synthesis environment with hydrocarbons (grease). The band at 1543 cm^{-1} is also assigned to bi-/carbonates.

TEM Microscopy. The TEM images of representative crystals of the HY and MgOHY samples are shown in Fig. 1, together with the reference MgO sample prepared with the same procedure. Unsupported MgO crystallizes in regular polyhedral

View Article Online
DOI: 10.1039/C8CP01788C

microcrystals ranging 150-300 nm in size (Fig. 2a). The MgOHY composite sample (Fig. 2c) does not contain neither this kind of particle nor any other detectable MgO separate phase, as further confirmed later by EDS and XRPD.

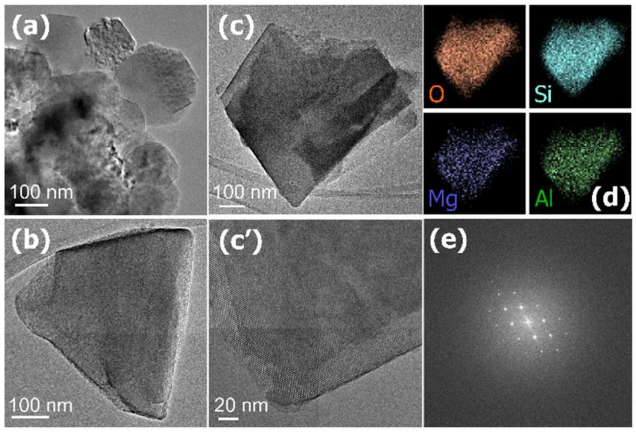

Fig. 2. TEM micrographs of (a) MgO, (b) HY and (c,c') MgOHY. (d) EDS maps obtained on the MgOHY particle reported in (c). Regions where the fluorescence photons have been collected for O (orange), Si (light blue), Mg (violet) and Al (green) elements are represented with different colors. (e) Diffraction pattern on a portion of MgOHY obtained by Fourier transform of (c').

MgOHY crystals have an irregular and diverse morphology, as usual for industrial zeolite samples, which reflects that of the parent zeolite (Fig. 2b). The distribution of MgO on the sample has been investigated also by means of EDS analysis. As an example, element maps for Si, Al, Mg and O for the MgOHY particle shown in Fig. 2b are presented in Fig. 2d. These maps show that the elemental concentration of Mg in the crystallite is uniform and comparable to that of the framework elements Si, Al and O. This indicates the absence of a separate MgO phase and suggests a uniform distribution of Mg within the pore structure of the material. The observed slight granularity of the maps is attributed to the sampling noise. Sampling on different particles allowed to determine that the concentration of Mg was uniform in the sample and an average atomic concentration for Mg of about 3% was obtained (MgO to HY weight ratio of 0.089 ± 0.01 or 8.2±1 wt%), that is very close to the expected value. The diffraction pattern obtained on a portion of Fig. 2c (part c') is reported in Fig. 2e. This pattern was identical to those obtained for HY sample. This can be taken as a further confirmation of the small dimension of the MgO clusters.

Nitrogen volumetry. The stability of the faujasite pore structure in the conditions adopted during the HY and the MgOHY syntheses was evaluated by means of nitrogen adsorption measurements at 77 K. This technique allows a complementary detection of structural modifications with respect to XRD, because it detects also the formation of amorphous or unordered features (e.g. mesopores).[64] The results are reported in Fig. 3 and Table 1. For what concerns HY, it is worth noticing that the HY sample has a higher surface area with respect to the starting NH_4Y (see Table **1**), as expected on the base of the decomposition of the ammonium group. Moreover, the HY surface area is almost coincident with its theoretical geometrical value. This result differs from previous reports in the literature[1,65] which described the occurrence of framework collapse in NH_4Y upon heating, with corresponding loss of surface area. The isotherms obtained for HY and MgOHY systems are reported in Fig. 3a as grey and blue curves respectively. Both the isotherms have a type Ia character,[46] typical of microporous materials. The fact that mesopores are not formed during MgOHY synthesis is qualitatively evident by the small hysteresis loop observed in the nitrogen isotherms (blue line in Fig. 3a) and from the pore size distributions (PSD) reported in Fig. 3b, indicating that all of the pore volume is in the micropore range. The two PSD are characterized by a peak at 11 Å, corresponding to the maximum diameter of a sphere inscribable in the zeolite supercage (11.2 Å).[66]

Table 1. Lanmguir surface area ($S_{Langmuir}$, $m^2\ g^{-1}$) and total pore volume calculated at p/p_0 = 0.97 (V_{tot}, in $cm^3\ g^{-1}$) and by means of the Langmuir analysis ($V_{Langmuir}$) of NH_4Y, HY and MgOHY. The area external to the micropores (S_{ext}, $m^2\ g^{-1}$) and micropore volume (V_{micro}, $cm^3\ g^{-1}$) calculated using the t-plot method, are also reported.

	$S_{Langmuir}$	S_{ext}	V_{tot}	$V_{Langmuir}$	V_{micro}
HY	888	56	0.38	0.31	0.29
MgOHY	786	25	0.31	0.28	0.26
NH_4Y	759	51	0.32	0.27	0.24

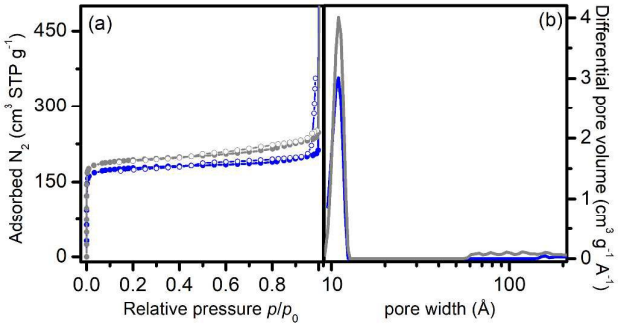

Fig. 3. (a) Volumetric N_2 adsorption/desorption isotherms obtained at 77 K and b) pore size distributions obtained by analysing the data using NLDFT (oxide, cylinder model) for HY (grey curve) and MgOHY (blue curve). Filled and empty circles of (a) refer to adsorption and desorption branches, respectively.

The loss of surface area upon the formation of the MgOHY composite is comparable with what expected considering the added weight of MgO and the associated pore volume loss (calculated 822 $m^2\ g^{-1}$ versus measured 786 $m^2\ g^{-1}$).

Although these two values may be considered coincident within the accuracy of the method, this discrepancy might be also explained with the fact that MgO particles are hosted inside the pores of the zeolite and that Mg incorporation exceeded the simple $2H^+ \rightarrow Mg^{2+}$ ion exchange, as verified by IR spectroscopy. In fact, considering the MgO bulk density (3.60 g cm^{-3}) and assuming a standard volume-area relationship, the MgO present in the channels would cause a decrease of 17 m^2

View Article Online
DOI: 10.1039/C8CP01788C

g^{-1}. The pore size distributions reported in Fig. 3b indicates that the decrease in surface area is imputed actually to a decrease in the micropore volume, as also suggested by the values obtained by the t-plot (see Table 2). It is worth noticing that the micropore volume obtained by the t-plot is only slightly lower than the pore volume obtained by expressing the Langmuir surface area as condensed gas volume ($V_{Langmuir}$). This confirm on one hand the high microporosity of the sample but also validates the use of the Harkins and Jura equation for these materials. A significant loss of external surface is observed with Mg incorporation (see Table 1 and isotherms in Fig. 3). The origin of this material modification is not clear, not being evident even in the microscopic analysis. It is here tentatively associated to physical loss of the smallest zeolite particles during the different phases of the MgOHY synthesis.

XRPD. The XRPD patterns of the activated HY and MgOHY materials, are reported in Figure S5 of ESI. The low strain and large crystallite domains characteristic of these materials is evident from the small FWHM of the peaks, also at high angles. In particular, the patterns of the HY zeolite and of the MgOHY composite are qualitatively identical. It is worth noting that the MgOHY sample lacks any extra peak associable with the presence of MgO or $Mg(OH)_2$, thus definitely excluding any segregation of Mg-related species.

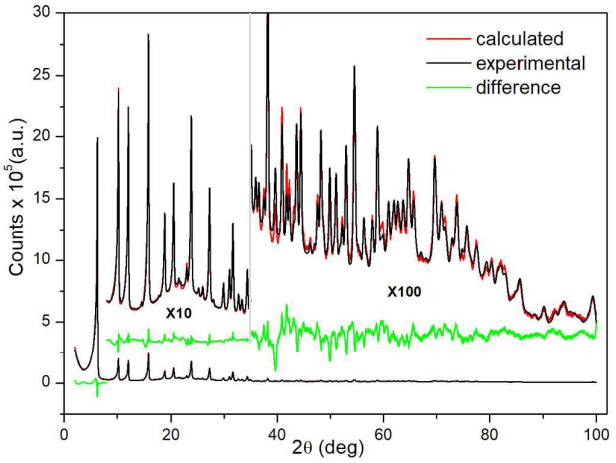

Fig. 4. Refinement of PXRD patterns of outgassed HYMgO. Black: experimental pattern, red: calculated pattern, and green: residual. Background: full scale pattern; insets: medium and high angles, scaled x10 and x100 respectively.

The two XRPD patterns, e.g. with and without MgO, were refined starting from the standard Y zeolite structure[67] without any adsorbed species or cations, according to the indications coming from chemical composition by the supplier, also confirmed by EDS analysis. The two patterns (see Fig. S5) show very small differences in peak intensities, as expected because of the lightness of magnesium (Z=12, approximately 10 electrons considering an Mg^{2+} ions) and its low concentration (lower than 3% in atoms). However, the reference outgassed Y zeolite showed a volume of 14688.4(7) $Å^3$ and a disagreement factor between the calculated and the experimental structure of 7%. Conversely, the refinement of the MgOHY XRPD without extra-framework species showed a remarkable volume decrease down to 14594.6(8) $Å^3$ and a much larger disagreement factor of 11%, indicating a detectable effect of MgO insertion within the framework, since adsorption on the surface of the crystallites would not affect lattice parameters. A decrease in the cell volume is often caused by the introduction of extra-framework species in zeolites, and specifically in the case of zeolite Y [63]. From a local viewpoint, the experimental cell edge (decrease from 24.49 for H-Y to 24.44 Å for MgOHY) is consistent with the contraction of the six-membered rings induced by the presence of Mg, as suggested also by modeling (see Fig. 6 and Fig. 7a and their discussion) and observed in the crystal structure, where the refined O-O distance in the six-membered ring changes from 5.09 in HY to 5.01 Å MgOHY.

EDS and IR analyses indicated that the unique differences between the two samples is the presence of MgO clusters. Both XRPD patterns were then analyzed searching for possible MgO locations by means of a simulated annealing procedure, as implemented in Topas TA. To avoid bias due to *a priori* information in the simulated annealing procedure, two separated Mg and O atoms, without any constraint were left free of moving fully independently in the whole cell, framework atom space included. In the Mg-impregnated sample, a Mg atom was located in the 6-member ring as shown in Fig. 5 with an occupancy per cell consistent with that suggested by EDS analysis, and the disagreement factor dropped down to 3.91% from initial 11%. The difference between the calculated (red line) and the experimental pattern (black line) is reported as green line in Fig. 4. The O atom was located close (2.77 Å) to the Mg atom, confirming the presence of MgO moieties. As a double check, the outgassed Y sample was subjected to the same procedure as reference but a much smaller disagreement factor improvement, reaching 4.43% from 7%, was observed. The six-member ring can be considered the preferred location of any adsorbed species (residual Na^+ ions, impurities and, when present, Mg^{2+}). The difference in occupancy, the change of the unit cell and the improvement of disagreement factor assure that the Mg^{2+} location is reliable. The Mg^{2+} location explains the shrinkage of the cell of the Mg-containing sample: Mg insertion causes the decrease of the six-member ring size and of the cage in general and the shrinkage is then transferred to the whole cell. The distance of Mg from framework oxygen atoms is 2.14 Å, larger than the expected standard Mg-O contact but it must be considered that the adopted symmetry constrains the disordered Mg and O atoms in special positions. At the same time, the symmetry imposes two close Mg^{2+} positions (see Fig. 5) with an unlikely short Mg-Mg contact. However, the low occupancy of magnesium assures that in the same unit cell only one of the two positions is occupied. The resulting Mg-O distance in the extraframework pair (2.77 Å) is larger than expected for a Mg-O bond. Beyond the well-known difficulty in assigning and locating disordered atoms with low occupancies from powder diffraction data, the two atoms must obey to the higher symmetry of the framework as often

View Article Online
DOI: 10.1039/C8CP01788C

observed in zeolites such as MFI.[68] All the Mg and O possible atom positions in the whole crystal are therefore mediated in the two average positions found in the Rietveld refinement. Moreover, the agreement factor changes very little and XRPD can hardly distinguish between the two possible locations, e.g. placing the O and Mg atoms as in Fig. 5 or inverting them). We conclude that these two positions may be regarded as partially-occupied (and symmetry-averaged) locations of MgO pairs. The Mg position in the 6-membered rings is close to ion-exchange position I' of zeolite Y: *x,x,x*; multiplicity 32, Wyckoff letter *e* ,site symmetry *3m,* 7,26 atoms per cell corresponding to 1.46(5)wt% Mg. Therefore, we can postulate that part of the Mg introduced by impregnation occupies ion-exchange positions.

However, it must be noticed that, given the Si/Al ratio and the Mg content of the material, the observed occupancy of the Mg sites does not account for all of the Mg present. Therefore, the presence of other MgO clusters need to be postulated. It can be concluded that, according to XRPD data Mg ions and/or MgO clusters are surely located close to the entrance of the six-membered ring in one of the possible positions available for Mg and O atoms. Only the Mg atoms close to and constrained by the six member rings show a degree of ordering enough large to be detected by XRPD. Disordered cluster, too large and irregular to obey to the high symmetry of the Y framework should be present to explain all the adsorbed Mg and the indication by IR spectroscopy. A further insight into these structures is obtained by means of the quantum mechanical models described below.

Modeling results. The screening of the energies and structures of the *isolated* (MgO) and *clustered* models over the different cage locations and Al proximities in the zeolite supercage provided a very broad range of energies and structures. Although a variety of $(MgO)_n$ models with n= 1,3,4,7 were studied, the following discussion will present only the results obtained for n=1 and n=4. This choice has several reasons. Firstly, these compositions allow to model ion exchange (n=1) and the behavior of the most stable gas phase cluster (n=4) upon encapsulation in zeolite Y. Secondly, only for n=4 we were able to explore systematically different locations in the zeolite supercage, a significant matter as we will discuss below. Finally, we observed for all cluster sizes, some recurrent topological/structural features, which are well represented by the $(MgO)_4$ family. The main structural and energetic results are shown in in Fig. 6, Fig. 7 and Table 2.

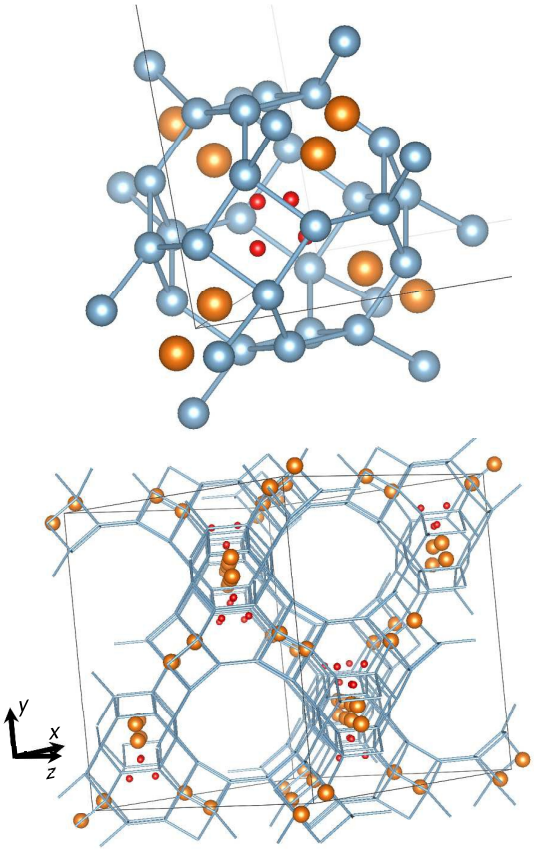

Fig. 5. Magnesium and oxygen location into the six-member ring (top) and within the zeolite unit cell (bottom), as obtained from Rietveld refinement of the MgOHY XRPD. Framework oxygen atoms are omitted. The color code is: light blue = Si or Al, orange = Mg, red = O. The two refined structures of the Y zeolite without and with MgO were deposited within the COD database with entry numbers 3000174 and 3000175.

Table 2. Relative energy (kJ mol^{-1} $cell^{-1}$) of the most stable possible structures for $(MgO)_4$ units hosted in HY zeolite. All energies are relative to the energy of the "open cube in supercage" structure. Structures are reported in Fig. 6 and Fig. 7. For each cluster the number of OH groups/bonds and the number of Al atoms in the framework rings closer to the clusters. In the case of the isolated MgO units, the counted OH groups correspond to four water molecules per cell, each coordinated to a Mg ion.

Structure type	E_{rel}	# OH	# Al atoms
cube in sodalite cage	-600.1	4	9
isolated Mg^{2+} (4 units)	-469.1	8[a]	8
open cube in supercage	0.0	2	3
cube in supercage	25.8	3	3
brucite-like in supercage	33.4	3	2

[a]Each Mg^{2+} ion is coordinated to one water molecule and then the –OH group reported here are H-O-H species unlike for the other structures where only Mg-O-H species are present.

View Article Online
DOI: 10.1039/C8CP01788C

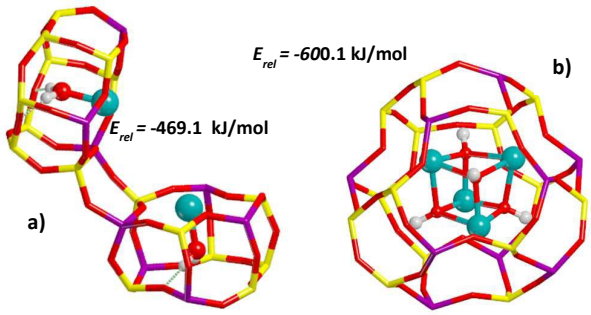

Fig. 6. Optimized structures of highly solvated models in the framework of HY zeolite as obtained at the B3LYP-D*/DZVP level: a) 4 isolated MgO moieties (only 2 are shown for clarity); b) $(MgO)_4$ cluster in the sodalite cage. (color code: Si=yellow, Al=violet, O=red, Mg=green). Energies are relative to the most stable structure in the supercage (see Table 2). Reaction with acidic protons forms water in a) and hydroxyls in b).

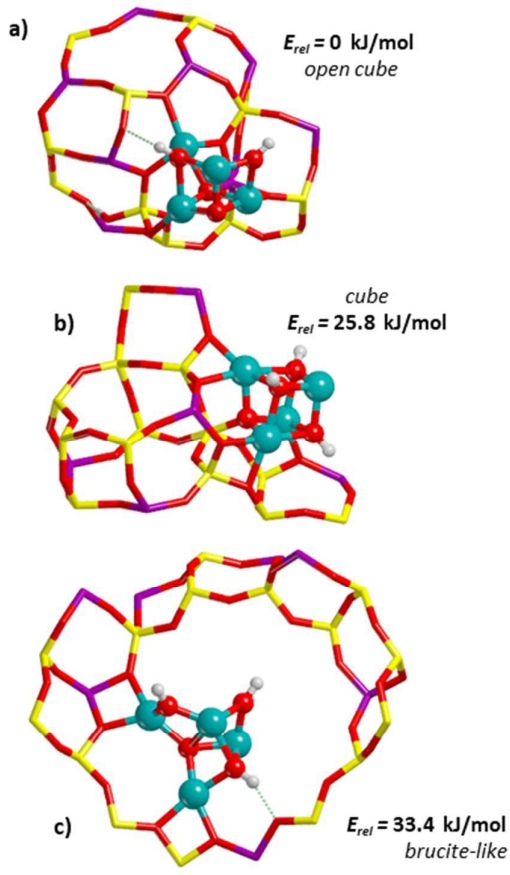

Fig. 7. Optimized structures of representative $(MgO)_4$ clusters in the framework of the HY zeolite as obtained at the B3LYP-D*/DZVP level (color code: Si=yellow, Al=violet, O=red, Mg=green). The numbers on the graph indicate the difference in energy per unit cell of the different models.

The models solvated by small cavities are by far the more stable. The lower energy structure is a hydrated $(MgOH)_4$ cube nested in the sodalite cage (Fig. 6b). The great stability of this structures owes to the formation of 4 OH groups and the high coordination of all Mg ions, which are relatively close to typical Mg coordination to 6-membered rings. The second more stable structure comprises four isolated MgO units inserted in double-6-ring cages, as shown in Fig. 6a. The oxygen atom of MgO captures two adjacent acidic protons to form a water molecule and the resulting site can be described as a hydrated Mg^{2+} ion in a typical ion exchange site. This is the only structure in wich the formation of H_2O is observed. The stability of this site is likely related to the highly coordinated Mg and the high energy of neutralization of the zeolite acidic protons by the basic MgO oxygen. The calculated interaction energy for the reaction (unbalanced for clarity):

$$HY + 4\ MgO \rightarrow 4\ Mg^{2+}\bullet H_2O\bullet Y$$

is -119.5 kJ/mol per MgO unit (considering a bulk MgO periodic crystal model). It is noteworthy that the structure containing single MgO units in the double-6-ring is obtained irrespective of the starting position of the MgO unit in both the supercage or sodalite cage.

The cluster models are all approximately 500 kJ mol^{-1} $cell^{-1}$ higher in energy (per unit cell of equal composition, see Table 2). This suggests that the formation of MgO clusters is significantly hindered for low Mg loadings, in favor of the ion exchange. When formed, the oxidic clusters display a variety of structural motifs shown in Fig. 7. We have adopted the lowest energy cluster as energy zero and screened the structures with energies lying within 100 kJ mol^{-1} $cell^{-1}$ from it for discussion and further investigation. Their structures are shown in Fig. 7a-c. The most stable *cluster* model (Fig. 7a) is a distorted cube where one edge has been elongated (*open cube*). This cluster sits on a 6-ring close to the 12-ring window outside the supercage. Distortion is apparently caused by two major interactions: 1) one Mg atom has been captured in the typical ion-exchange location by an Al-rich six-membered ring; 2) one O atom has captured an acidic proton to form a hydroxy group. The next more stable structure (+25.8 kJ mol^{-1} $cell^{-1}$) is an almost undistorted *cube* bearing three hydroxyls. This almost perfect cube is shared between two four-rings and it points inside the supercage. Its stability is likely due not only to intrinsic stability of cubic clusters observed in the gas phase, but also to the high energy of formation of OH groups from the basic cluster and acidic Brønsted sites. Species as those modeled by the *open cube* and the *cube* clusters are those responsible for the EXAFS and XANES results reported by Tsuji et al.[33] Interestingly, a third type of structure is found with similar energy (Fig. 7d, +33.4 kJ mol^{-1} $cell^{-1}$), also favoured by the formation of three hydroxy groups. It has a completely different structure: the initial cube structure is completely lost due to the strong interaction with the zeolite pore wall and the formation of three hydroxy groups. This cluster occupies the 12-ring window plane, with two Mg ions coordinated to the Al atoms of the ring. This structure bears some similarity with the local structure of the layered hydroxide *brucite* $Mg(OH)_2$ and in particular with its (110) surface[69]. Given the peculiar stability of this low-coordinated fragment, we have investigated its possible stabilization by solvation in the sodalite cage. Interestingly, optimization of this cluster in the sodalite cage leads to the formation of the cubic cluster described above (Fig. 6b).

View Article Online
DOI: 10.1039/C8CP01788C

The main factors determining the structural stability of the MgOHY composite models appear to be the interaction of basic oxygen atoms of the clusters with the acidic protons of the zeolite (with the formation of –OH species) and the interaction of Mg ions with Al-containing zeolite rings. This is clearly seen from the data of Table 2, where the number of O-H bonds formed upon interaction of the cluster with the zeolite, and the number of Al atoms in close contact with the MgO cluster are tabulated. Open, less coordinated structures are found in the supercage, but not in the small cages, where compact structures can be fully coordinated by the zeolite framework.

Discussion. Interestingly, in spite of the very high stability of the isolated MgO structures, where Mg attains atomic dispersion in the zeolite, not all of the available sites for ion exchange are occupied in the composite, as evidenced by the persistence of the acidic OH band in the infrared spectra of the composite (see Fig. 1). The difficulty in attaining full ion exchange with divalent cations is well documented[70] and it is attributed to both topological restrictions and the low diffusivity of hydrated divalent cations. Therefore, we hypothesize a formation mechanism with two stages. Initially, partial ion exchange with the Mg-nitrate solution occurs, limited by the availability of sites bearing two neighboring Al atoms and by the limited mobility of the large and stable $[Mg(H_2O)_6]^{2+}$ ions. In this phase, the very stable *ion exchange* sites are formed and possibly also some "*cube in sodalite cage*" structures, subject to diffusion limitations. (Fig.6). Upon dehydration and thermal treatment, the remaining magnesium hydroxide/oxide clusters form. The structures of these clusters arises from the balance between: a) stability of the cluster itself (with cubes being favored); b) solvation of the cluster by the zeolite framework, and; c)acid-base reactions with formation of magnesium hydroxide fragments or water.

Our simulation results indicate that, despite the large number of theoretical possible structures, these constrains lead to a limited number of structure types, showing distinctive structural features. These structural motifs locally echoes well-known zeolite or bulk oxide/hydroxide features. We are aware of the fact that our investigation covers only a fraction of the theoretically possible situations. However, we observed that a large number of them converge to a limited number of these characteristic structural motifs. These motifs, randomly located in the zeolite cavities may be responsible for the distinctive reactivity of basic zeolites. These results are in agreement with what predicted by Pydko et al for Al_xO_y clusters[28] and further demonstrate the role of framework solvation in the stabilization of oxide clusters in zeolites. Open low coordinated structures similar to our "brucite-like" structures are also predicted by Larin et al.[31] for Mg_2O_n clusters, but with one notable difference: we do not observe the formation of short O-O distances. However, this might be explained by the fact that residual zeolite acidity is explicitly taken in account in our models, causing the most basic oxygens of MgO clusters to react with the acidic protons, forming OH groups or water. The persistence of this stable OH population also at relatively high temperature is in agreement with the IR spectra (Fig.1)

In order to provide an initial characterization for the proposed structures, their reactivity toward CO_2 has been investigated. CO_2 is in fact both an "imperfect probe molecule"[12] probing both acid and basic sites and an interesting substrate for technological reasons. The detailed experimental study of the interaction of CO_2 with the material at technically interesting conditions will be reported in a separate paper. Adsorption of CO_2 on the five structures listed in Table 2 has been modeled. Initial coordinates of the models were manually constructed by linearly coordinating the CO_2 molecule to the least coordinated Mg atom of the cluster. An attempt to start with CO_2 coordinated through the carbon atom to the least coordinated oxygen (as frequently observed on MgO defects) lead to the same optimized geometries and was not further investigated. The structures of the MgOHY-CO_2 adducts are shown in Fig. 8, together with the calculated energies of adsorption. We do not report the results of CO_2 adsorption on the cube in sodalite structure, for several reasons. Firstly, experimental evidences[12] exclude the permeability of the sodalite cage to CO_2. Secondly, there is not enough room to form molecular complexes with CO_2 in the sodalite occupied by $(MgO)_4$ clusters due to the fact that there is not enouth room for molecular CO_2 in the sodalite, as confirmed by our modeling attempts. Adsorption on the *isolated MgO* model leads to an interesting coordination of the CO_2 molecules to two Mg sites in adjacent 6-membered rings (Fig. 8a), with an adsorption energy per CO_2 molecule of -65.8 kJ/mol. Interestingly, the existence of a similar bridging structure had been previously predicted by Thang et al.[43] on the basis of spectroscopic experiments. However, the structure proposed based on the spectroscopic evidence is likely located in the supercage, while our model has the odd feature of having the CO_2 molecule inside a sodalite cage. A similar coordination geometry is possible also in the supercage, but it has not been modeled in this work, due the computational cost. Nevertheless, it is experimentally well-known that extraframework ions are highly mobile in response to adsorbates in Y zeolites[13]. The cubic clusters form linear adducts with CO_2, with adsorption energies ranging from -66.2kJ/mol (structure not shown) to -104.2 kJ/mol (Fig. 8c) and minor modification of both the cluster and the CO_2 molecules. A similar geometry, with a very similar energy of adsorption, was also obtained for the *brucite* model (Fig. 8d). On the contrary, adsorption on the *open cube* model leads to a rearrangement of CO_2 and the cluster with formation of an HCO_3^- ion (Fig. 8b). Despite the extensive molecular reorganization, the reaction energy is only -18.6 kJ/mol, probably due to the high deformation energy necessary for the rearrangement.

The cause of stabilization of the complexes is a typical Lewis acid–Lewis base interaction. The strength of the interaction can be further increased by synergistic hydrogen bonds, involving one of the oxygens of CO_2. Chemisorption with formation of carbonates, which we observe on the *open cube* model only, seems to require a specific site stabilizing the ion. In the case of Fig 8b, stabilization may arise from the insertion

View Article Online
DOI: 10.1039/C8CP01788C

of the carbonate in the open cube structure with concomitant hydrogen bonding with the zeolite framework.

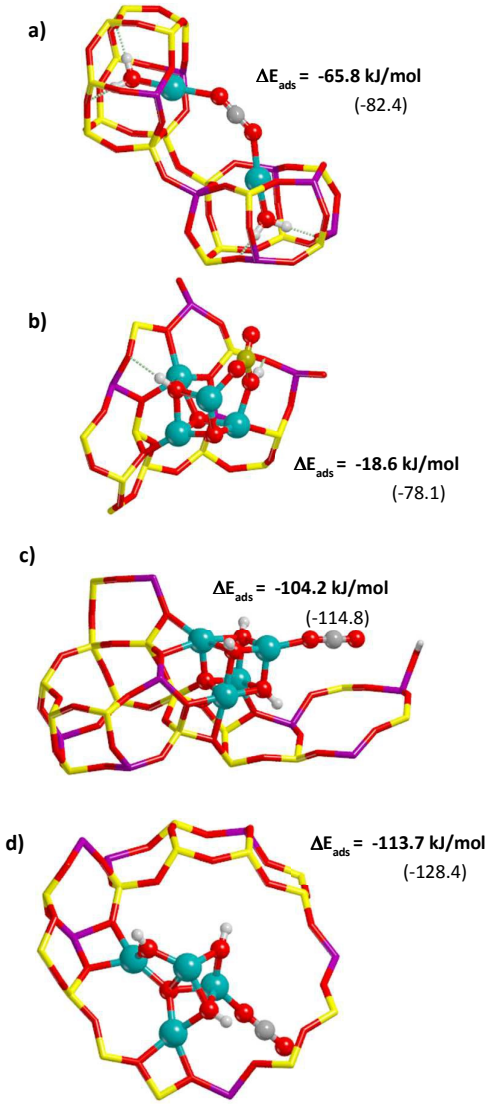

Fig. 8. Optimized structures and adsorption energies of the adducts formed by CO_2 on MgOHY models reported in Fig. 6 and Fig. 7. Numbers in bold refer to results obtained with the B3LYP-D* method using the TZVP basis set, while number in parentheses were obtained with DZVP (color code:Si=yellow, Al=violet, O=red, Mg=dark green, C=grey).

From Fig. 8b, a lower stability of the carbonate/bicarbonate-like species in MgOHY than in bulk MgO can be expected, because of their low coordination environment. This is in agreement with previous experimental results on CO_2 adsorption on basic Mg-zeolites[33] where a desorption temperature, well below the typical decomposition temperature of carbonates, has been reported.

Conclusions

In summary, we have synthesized a "superbasic" HY/MgO zeolite/oxide (or zeolite/hydroxide) nanocomposite with high MgO content, high crystallinity and highly dispersed Mg sites, and we have investigated the active sites of the material with a synergic use of experimental data and computational models. We provide evidence that the material comprises clusters of magnesium oxide and hydroxide hosted by the microporous zeolite framework. The location and structure of the Mg-containing clusters have been studied by Rietveld refinement of X-ray powder diffraction data, combined with high quality quantum mechanical simulations. The refinement has shown the presence of magnesium and oxygen atoms consistent with isolated (MgO) units. Occupancy of these sites explain only part of the Mg present in the sample, being the technique blind to disordered low symmetry clusters. Experimental evidences prompted for the presence of additional Mg-containing species in the pores, whose nature has been studied by modelling. Periodic models of $(MgO)_n$ clusters in different locations of the zeolite structure were investigated. Two families of possible sites were identified: highly solvated clusters in small pores and less coordinated moieties in the supercage. Solvated sites are by far more stable and ordered. However, their formation is limited by topological and steric constrains, giving rise also to the formation of less solvated clusters in the supercages. The structures of the very stable $(MgO)_4$ clusters were studied systematically and they displayed structural features common to all clusters studied. Their stability appears to be regulated by the ability of Mg ions to interact with the negative pore walls and by the formation of Mg-OH species by interaction of MgO with remaining acidic protons. A certain preference for cubic structures (the most stable in the gas phase) is also retained by embedded clusters in agreement with EXAFS data reported previously on similar systems. The most stable structures are characterized by extensive solvation by the framework, as observed in isolated MgO units in double-6-membered rings and by $(MgO)_4$ in the sodalite cage. The latter, although very stable, might be irrelevant for adsorption properties due to its inaccessibility. A brucite-like cluster was also obtained, possessing a *quasi* 2D structure developing in the plane of the 12-ring window that serves as access to the supercage. Its stability is associated to the simultaneous interaction with three oxygens of Al-O bond present in the ring.

The reactivity of four representative models with CO_2 has been modelled. CO_2 forms very stable linear end-on adducts with low coordinated Mg ions in most cases. Ion exchange sites give rise to bridge bidentate complexes in agreement with previous spectroscopic findings. The formation of hydrogen-carbonates is observed only on specific sites.

These findings constitutes an unprecedented level of detail in the characterization of basic zeolites, with a great impact on the understanding of their adsorptive and catalytic properties.

Acknowledgements

Federica Franconieri is acknowledged for TEM measurements. Gianmario Martra is acknowledged for fruitful discussions. Part

View Article Online
DOI: 10.1039/C8CP01788C

of the simulations were performed on resources provided by UNINETT Sigma2 - the National Infrastructure for High Performance Computing and Data Storage in Norway, under project number NN9381K.

Notes and references

1. J. Čejka, R. Morris and P. Nachtigall, *Zeolites in Catalysis: Properties and Applications*, Royal Society of Chemistry, 2017.
2. H. Hattori, *Chem. Rev.*, 1995, **95**, 537-558.
3. G. Busca, *Industrial & Engineering Chemistry Research*, 2009, **48**, 6486-6511.
4. T. H. Bae, M. R. Hudson, J. A. Mason, W. L. Queen, J. J. Dutton, K. Sumida, K. J. Micklash, S. S. Kaye, C. M. Brown and J. R. Long, *Energy Environ. Sci.*, 2013, **6**, 128-138.
5. M. Tagliabue, D. Farrusseng, S. Valencia, S. Aguado, U. Ravon, C. Rizzo, A. Corma and C. Mirodatos, *Chem. Eng. J.*, 2009, **155**, 553-566.
6. B. Puertolas, T. C. Keller, S. Mitchell and J. Perez-Ramirez, *Appl. Catal. B-Environ.*, 2016, **184**, 77-86.
7. L. Zhang, T. N. Pham, J. Faria, D. Santhanaraj, T. Sooknoi, Q. H. Tan, Z. Zhao and D. E. Resasco, *ChemSusChem*, 2016, **9**, 736-748.
8. I. Graca, D. Iruretagoyena and D. Chadwick, *Appl. Catal. B-Environ.*, 2017, **206**, 434-443.
9. G. M. Lari, K. Desai, C. Mondelli and J. Perez-Ramirez, *Catal. Sci. Technol.*, 2016, **6**, 2706-2714.
10. P. Gao, S. G. Li, X. N. Bu, S. S. Dang, Z. Y. Liu, H. Wang, L. S. Zhong, M. H. Qiu, C. G. Yang, J. Cai, W. Wei and Y. H. Sun, *Nature Chemistry*, 2017, **9**, 1019-1024.
11. J. Wei, Q. J. Ge, R. W. Yao, Z. Y. Wen, C. Y. Fang, L. S. Guo, H. Y. Xu and J. Sun, *Nature Communications*, 2017, **8**.
12. R. A. Schoonheydt, P. Geerlings, E. A. Pidko and R. A. van Santen, *Journal of Materials Chemistry*, 2012, **22**, 18705-18717.
13. S. Bordiga, C. Lamberti, F. Bonino, A. Travert and F. Thibault-Starzyk, *Chemical Society Reviews*, 2015, **44**, 7262-7341.
14. D. Barthomeuf, *Catal. Rev.*, 1996, **38**, 521-612.
15. T. K. Phung and G. Busca, *Applied Catalysis a-General*, 2015, **504**, 151-157.
16. J. G. Vitillo, *RSC Adv.*, 2015, **5**, 36192-36239.
17. M. B. Jensen, L. G. M. Pettersson, O. Swang and U. Olsbye, *Journal of Physical Chemistry B*, 2005, **109**, 16774-16781.
18. J. M. C. Plane and C. L. Whalley, *Journal of Physical Chemistry A*, 2012, **116**, 6240-6252.
19. D. van Heijnsbergen, G. von Helden, G. Meijer and M. A. Duncan, *Journal of Chemical Physics*, 2002, **116**, 2400-2406.
20. P. J. Ziemann and A. W. Castleman, *Zeitschrift Fur Physik D-Atoms Molecules and Clusters*, 1991, **20**, 97-99.
21. P. J. Ziemann and A. W. Castleman, *Journal of Chemical Physics*, 1991, **94**, 718-728.
22. A. I. Boldyrev and J. Simons, *Journal of Physical Chemistry*, 1996, **100**, 8023-8030.
23. S. Moukouri and C. Noguera, *Zeitschrift Fur Physik D-Atoms Molecules and Clusters*, 1993, **27**, 79-88.
24. J. M. Recio, R. Pandey, A. Ayuela and A. B. Kunz, *Journal of Chemical Physics*, 1993, **98**, 4783-4792.
25. E. delaPuente, A. Aguado, A. Ayuela and J. M. Lopez, *Physical Review B*, 1997, **56**, 7607-7614.
26. X. Lu, X. Xu, N. Q. Wang and Q. N. Zhang, *International Journal of Quantum Chemistry*, 1999, **73**, 377-386.
27. K. Kwapien, M. Sierka, J. Dobler, J. Sauer, M. Haertelt, A. Fielicke and G. Meijer, *Angewandte Chemie-International Edition*, 2011, **50**, 1716-1719.
28. E. A. Pidko, J. Xu, B. L. Mojet, L. Lefferts, I. R. Subbotina, V. B. Kazansky and R. A. van Santen, *Journal of Physical Chemistry B*, 2006, **110**, 22618-22627.
29. R. Bulanek, I. Voleska, E. Ivanova, K. Hadjiivanov and P. Nachtigall, *Journal of Physical Chemistry C*, 2009, **113**, 11066-11076.
30. A. A. Rybakov, A. V. Larin, G. M. Zhidomirov, D. N. Trubnikov and D. P. Vercauteren, *Computational and Theoretical Chemistry*, 2011, **964**, 108-115.
31. A. V. Larin, A. A. Rybakov, G. M. Zhidomirov, A. Mace, A. Laaksonen and D. P. Vercauteren, *Journal of Catalysis*, 2011, **281**, 212-221.
32. A. Abou-Kais, C. Mirodatos, J. Massardier, D. Barthomeuf and J. C. Vedrine, *The Journal of Physical Chemistry*, 1977, **81**, 397-402.
33. H. Tsuji, F. Yagi, H. Hattori, H. Kita, J. W. Hightower, J. C. Vedrire, W. K. Hall, D. Kallo, S. Coluccia and I. Kiricsi, *Studies in Surface Science and Catalysis*, 1993, **75**, 1171-1183.
34. T. Duren, Y. S. Bae and R. Q. Snurr, *Chemical Society Reviews*, 2009, **38**, 1237-1247.
35. S. Grimme, *Journal of Computational Chemistry*, 2004, **25**, 1463-1473.
36. S. Grimme, *Journal of Computational Chemistry*, 2006, **27**, 1787-1799.
37. S. Grimme, J. Antony, S. Ehrlich and H. Krieg, *Journal of Chemical Physics*, 2010, **132**.
38. M. Rapacioli, F. Spiegelman, D. Talbi, T. Mineva, A. Goursot, T. Heine and G. Seifert, *Journal of Chemical Physics*, 2009, **130**.
39. U. Zimmerli, M. Parrinello and P. Koumoutsakos, *Journal of Chemical Physics*, 2004, **120**, 2693-2699.
40. B. Civalleri, C. M. Zicovich-Wilson, L. Valenzano and P. Ugliengo, *Crystengcomm*, 2008, **10**, 405-410.
41. P. Ugliengo, C. M. Zicovich-Wilson, S. Tosoni and B. Civalleri, *Journal of Materials Chemistry*, 2009, **19**, 2564-2572.
42. B. Civalleri, L. Maschio, P. Ugliengo and C. M. Zicovich-Wilson, *Physical Chemistry Chemical Physics*, 2010, **12**, 6382-6386.
43. H. V. Thang, L. Grajciar, P. Nachtigall, O. Bludsky, C. O. Arean, E. Frydova and R. Bulanek, *Catalysis Today*, 2014, **227**, 50-56.
44. D. C. Sorescu, J. Lee, W. A. Al-Saidi and K. D. Jordan, *Journal of Chemical Physics*, 2011, **134**.
45. K. D. Vogiatzis, W. Klopper and J. Friedrich, *Journal of Chemical Theory and Computation*, 2015, **11**, 1574-1584.
46. S. J. Gregg and K. S. W. Sing, *Adsorption, surface area and porosity (2nd ed.)*, Academic Press Inc., London, 1982.
47. I. Langmuir, *J. Am. Chem. Soc.*, 1918, **40**, 1361–1403.
48. J. P. Olivier, *J. Por. Mater.*, 1995, **2**, 9-17.
49. A. Coelho, *Journal of Applied Crystallography*, 2005, **38**, 455-461.

View Article Online
DOI: 10.1039/C8CP01788C

50. C. F. Macrae, P. R. Edgington, P. McCabe, E. Pidcock, G. P. Shields, R. Taylor, M. Towler and J. van de Streek, *Journal of Applied Crystallography*, 2006, **39**, 453-457.
51. K. Momma and F. Izumi, *Journal of Applied Crystallography*, 2011, **44**, 1272-1276.
52. R. E. Fletcher, S. L. Ling and B. Slater, *Chemical Science*, 2017, **8**, 7483-7491.
53. M. Czjzek, H. Jobic, A. N. Fitch and T. Vogt, *Journal of Physical Chemistry*, 1992, **96**, 1535-1540.
54. A. Erba, J. Baima, I. Bush, R. Orlando and R. Dovesi, *Journal of Chemical Theory and Computation*, 2017, **13**, 5019-5027.
55. W. T. Yang, R. G. Parr and C. T. Lee, *Physical Review A*, 1986, **34**, 4586-4590.
56. R. Nada, J. B. Nicholas, M. I. McCarthy and A. C. Hess, *International Journal of Quantum Chemistry*, 1996, **60**, 809-820.
57. M. Catti, G. Valerio, R. Dovesi and M. Causa, *Physical Review B*, 1994, **49**, 14179-14187.
58. L. Valenzano, Y. Noel, R. Orlando, C. M. Zicovich-Wilson, M. Ferrero and R. Dovesi, *Theoretical Chemistry Accounts*, 2007, **117**, 991-1000.
59. T. Bredow, K. Jug and R. A. Evarestov, *Physica Status Solidi B-Basic Solid State Physics*, 2006, **243**, R10-R12.
60. R. Dovesi, G. Ermondi, E. Ferrero, C. Pisani and C. Roetti, *Phys. Rev. B*, 1984, **29**, 3591.
61. C. Gatti, V. R. Saunders and C. Roetti, *Journal of Chemical Physics*, 1994, **101**, 10686-10696.
62. P. Ugliengo and A. Damin, *Chemical Physics Letters*, 2003, **370**, 589-589.
63. C. Mirodatos, P. Pichat and D. Barthomeuf, *J. Phys. Chem.*, 1976, **80**, 1335-1342.
64. J. G. Vitillo and S. Bordiga, *Mater. Chem. Front.*, 2017, **1**, 444-448.
65. J. B. Condon, *Surface Area and Porosity Determinations by Physisorption*, Elsevier Science, 1st edn., 2006.
66. http://www.iza-structure.org/databases/.
67. G. Agostini, C. Lamberti, L. Palin, M. Milanesio, N. Danilina, B. Xu, M. Janousch and J. A. van Bokhoven, *Journal of the American Chemical Society*, 2010, **132**, 667-678.
68. L. Palin, C. Lamberti, Å. Kvick, F. Testa, R. Aiello, M. Milanesio and D. Viterbo, *The Journal of Physical Chemistry B*, 2003, **107**, 4034-4042.
69. T. Fornaro, J. Brucato, C. Dimitri, A. Sverjensky, R. M. Hazen, R. Brunetto, M. D'Amore and V. Barone, *Journal*, 2018.
70. K. R. Franklin and R. P. Townsend, *Journal of the Chemical Society-Faraday Transactions I*, 1988, **84**, 2755-2770.

View Article Online
DOI: 10.1039/C8CP01788C

Journal Name

ARTICLE

1. J. Čejka, R. Morris and P. Nachtigall, *Zeolites in Catalysis: Properties and Applications*, Royal Society of Chemistry, 2017.
2. H. Hattori, *Chem. Rev.*, 1995, **95**, 537-558.
3. G. Busca, *Ind. Eng. Chem. Res.*, 2009, **48**, 6486-6511.
4. T. H. Bae, M. R. Hudson, J. A. Mason, W. L. Queen, J. J. Dutton, K. Sumida, K. J. Micklash, S. S. Kaye, C. M. Brown and J. R. Long, *Energy Environ. Sci.*, 2013, **6**, 128-138.
5. M. Tagliabue, D. Farrusseng, S. Valencia, S. Aguado, U. Ravon, C. Rizzo, A. Corma and C. Mirodatos, *Chem. Eng. J.*, 2009, **155**, 553-566.
6. B. Puertolas, T. C. Keller, S. Mitchell and J. Perez-Ramirez, *Appl. Catal. B-Environ.*, 2016, **184**, 77-86.
7. L. Zhang, T. N. Pham, J. Faria, D. Santhanaraj, T. Sooknoi, Q. H. Tan, Z. Zhao and D. E. Resasco, *ChemSusChem*, 2016, **9**, 736-748.
8. I. Graca, D. Iruretagoyena and D. Chadwick, *Appl. Catal. B-Environ.*, 2017, **206**, 434-443.
9. G. M. Lari, K. Desai, C. Mondelli and J. Perez-Ramirez, *Catal. Sci. Technol.*, 2016, **6**, 2706-2714.
10. P. Gao, S. G. Li, X. N. Bu, S. S. Dang, Z. Y. Liu, H. Wang, L. S. Zhong, M. H. Qiu, C. G. Yang, J. Cai, W. Wei and Y. H. Sun, *Nat. Chem.*, 2017, **9**, 1019-1024.
11. J. Wei, Q. J. Ge, R. W. Yao, Z. Y. Wen, C. Y. Fang, L. S. Guo, H. Y. Xu and J. Sun, *Nat. Commun.*, 2017, **8**.
12. S. Bordiga, C. Lamberti, F. Bonino, A. Travert and F. Thibault-Starzyk, *Chem. Soc. Rev.*, 2015, **44**, 7262-7341.
13. D. Barthomeuf, *Catal. Rev.*, 1996, **38**, 521-612.
14. T. K. Phung and G. Busca, *Appl. Catal. A*, 2015, **504**, 151-157.
15. J. G. Vitillo, *RSC Adv.*, 2015, **5**, 36192-36239.
16. M. B. Jensen, L. G. M. Pettersson, O. Swang and U. Olsbye, *J. Phys. Chem. B*, 2005, **109**, 16774-16781.
17. J. M. C. Plane and C. L. Whalley, *J. Phys. Chem. A*, 2012, **116**, 6240-6252.
18. D. van Heijnsbergen, G. von Helden, G. Meijer and M. A. Duncan, *J. Chem. Phys.*, 2002, **116**, 2400-2406.
19. P. J. Ziemann and A. W. Castleman, *Z.Phys. D*, 1991, **20**, 97-99.
20. P. J. Ziemann and A. W. Castleman, *J.Chem.Phys.*, 1991, **94**, 718-728.
21. A. I. Boldyrev and J. Simons, *J.Phys. Chem.*, 1996, **100**, 8023-8030.
22. S. Moukouri and C. Noguera, *Z. Phys. D*, 1993, **27**, 79-88.
23. J. M. Recio, R. Pandey, A. Ayuela and A. B. Kunz, *J. Chem. Phys.*, 1993, **98**, 4783-4792.
24. E. delaPuente, A. Aguado, A. Ayuela and J. M. Lopez, *Phys. Rev. B*, 1997, **56**, 7607-7614.
25. X. Lu, X. Xu, N. Q. Wang and Q. N. Zhang, *Int. J. Quantum Chem.*, 1999, **73**, 377-386.
26. K. Kwapien, M. Sierka, J. Dobler, J. Sauer, M. Haertelt, A. Fielicke and G. Meijer, *Angew. Chem. Int. Ed.*, 2011, **50**, 1716-1719.
27. R. Bulanek, I. Voleska, E. Ivanova, K. Hadjiivanov and P. Nachtigall, *J. Phys. Chem. C*, 2009, **113**, 11066-11076.
28. A. Abou-Kais, C. Mirodatos, J. Massardier, D. Barthomeuf and J. C. Vedrine, *J. Phys. Chem.*, 1977, **81**, 397-402.
29. H. Tsuji, F. Yagi, H. Hattori, H. Kita, J. W. Hightower, J. C. Vedrire, W. K. Hall, D. Kallo, S. Coluccia and I. Kiricsi, *Stud. Surf. Sci. Catal.*, 1993, **75**, 1171-1183.
30. T. Duren, Y. S. Bae and R. Q. Snurr, *Chem. Soc. Rev.*, 2009, **38**, 1237-1247.
31. S. Grimme, *J. Comput. Chem.*, 2004, **25**, 1463-1473.
32. S. Grimme, *J. Comput. Chem.*, 2006, **27**, 1787-1799.
33. S. Grimme, J. Antony, S. Ehrlich and H. Krieg, *J. Chem. Phys.*, 2010, **132**.
34. M. Rapacioli, F. Spiegelman, D. Talbi, T. Mineva, A. Goursot, T. Heine and G. Seifert, *J. Chem. Phys.*, 2009, **130**.
35. U. Zimmerli, M. Parrinello and P. Koumoutsakos, *J. Chem. Phys.*, 2004, **120**, 2693-2699.
36. B. Civalleri, C. M. Zicovich-Wilson, L. Valenzano and P. Ugliengo, *Crystengcomm*, 2008, **10**, 405-410.
37. P. Ugliengo, C. M. Zicovich-Wilson, S. Tosoni and B. Civalleri, *J. Mater. Chem.*, 2009, **19**, 2564-2572.
38. B. Civalleri, L. Maschio, P. Ugliengo and C. M. Zicovich-Wilson, *PCCP*, 2010, **12**, 6382-6386.
39. H. V. Thang, L. Grajciar, P. Nachtigall, O. Bludsky, C. O. Arean, E. Frydova and R. Bulanek, *Catal. Today*, 2014, **227**, 50-56.
40. D. C. Sorescu, J. Lee, W. A. Al-Saidi and K. D. Jordan, *J. Chem. Phys.*, 2011, **134**.
41. K. D. Vogiatzis, W. Klopper and J. Friedrich, *J. Chem. Theory Comput.*, 2015, **11**, 1574-1584.
42. S. J. Gregg and K. S. W. Sing, *Adsorption, surface area and porosity (2nd ed.)*, Academic Press Inc., London, 1982.
43. I. Langmuir, *J. Am. Chem. Soc.*, 1918, **40**, 1361–1403.
44. J. P. Olivier, *J. Por. Mater.*, 1995, **2**, 9-17.
45. A. Coelho, *J. Appl. Crystallogr.*, 2005, **38**, 455-461.
46. C. F. Macrae, P. R. Edgington, P. McCabe, E. Pidcock, G. P. Shields, R. Taylor, M. Towler and J. van de Streek, *J. Appl. Crystallogr.*, 2006, **39**, 453-457.
47. K. Momma and F. Izumi, *J. Appl. Crystallogr.* 2011, **44**, 1272-1276.
48. R. E. Fletcher, S. L. Ling and B. Slater, *Chem. Sci.*, 2017, **8**, 7483-7491.
49. M. Czjzek, H. Jobic, A. N. Fitch and T. Vogt, *J.Phys. Chem.*, 1992, **96**, 1535-1540.
50. A. Erba, J. Baima, I. Bush, R. Orlando and R. Dovesi, *J. Chem. Theory Comput.*, 2017, **13**, 5019-5027.
51. W. T. Yang, R. G. Parr and C. T. Lee, *Phys. Rev. A*, 1986, **34**, 4586-4590.
52. R. Nada, J. B. Nicholas, M. I. McCarthy and A. C. Hess, *Int. J. Quantum Chem.*, 1996, **60**, 809-820.
53. M. Catti, G. Valerio, R. Dovesi and M. Causa, *Phys. Rev. B*, 1994, **49**, 14179-14187.
54. L. Valenzano, Y. Noel, R. Orlando, C. M. Zicovich-Wilson, M. Ferrero and R. Dovesi, *Theor. Chem. Acc.*, 2007, **117**, 991-1000.
55. T. Bredow, K. Jug and R. A. Evarestov, *Phys. Status Solidi B*, 2006, **243**, R10-R12.
56. R. Dovesi, G. Ermondi, E. Ferrero, C. Pisani and C. Roetti, *Phys. Rev. B*, 1984, **29**, 3591.

View Article Online
DOI: 10.1039/C8CP01788C

57. C. Gatti, V. R. Saunders and C. Roetti, *J. Chem. Phys.*, 1994, **101**, 10686-10696.
58. P. Ugliengo and A. Damin, *Chem. Phys. Lett.*, 2003, **370**, 589-589.
59. C. Mirodatos, P. Pichat and D. Barthomeuf, *J. Phys. Chem.*, 1976, **80**, 1335-1342.
60. J. G. Vitillo and S. Bordiga, *Mater. Chem. Front.*, 2017, **1**, 444-448.
61. J. B. Condon, *Surface Area and Porosity Determinations by Physisorption*, Elsevier Science, 1st edn., 2006.
62. http://www.iza-structure.org/databases/.
63. G. Agostini, C. Lamberti, L. Palin, M. Milanesio, N. Danilina, B. Xu, M. Janousch and J. A. van Bokhoven, *J. Am. Chem. Soc.*, 2010, **132**, 667-678.
64. L. Palin, C. Lamberti, Å. Kvick, F. Testa, R. Aiello, M. Milanesio and D. Viterbo, *J. Phys. Chem. B*, 2003, **107**, 4034-4042.
65. T. Fornaro, J. Brucato, C. Dimitri, A. Sverjensky, R. M. Hazen, R. Brunetto, M. D'Amore and V. Barone, *Astrobiology*, (accepted) 2018.
66. K. R. Franklin and R. P. Townsend, *J. Chem. Soc. Faraday Trans.*, 1988, **84**, 2755-2770.

View Article Online
DOI: 10.1039/C8CP01788C

Journal Name

ARTICLE

TOC Image and text

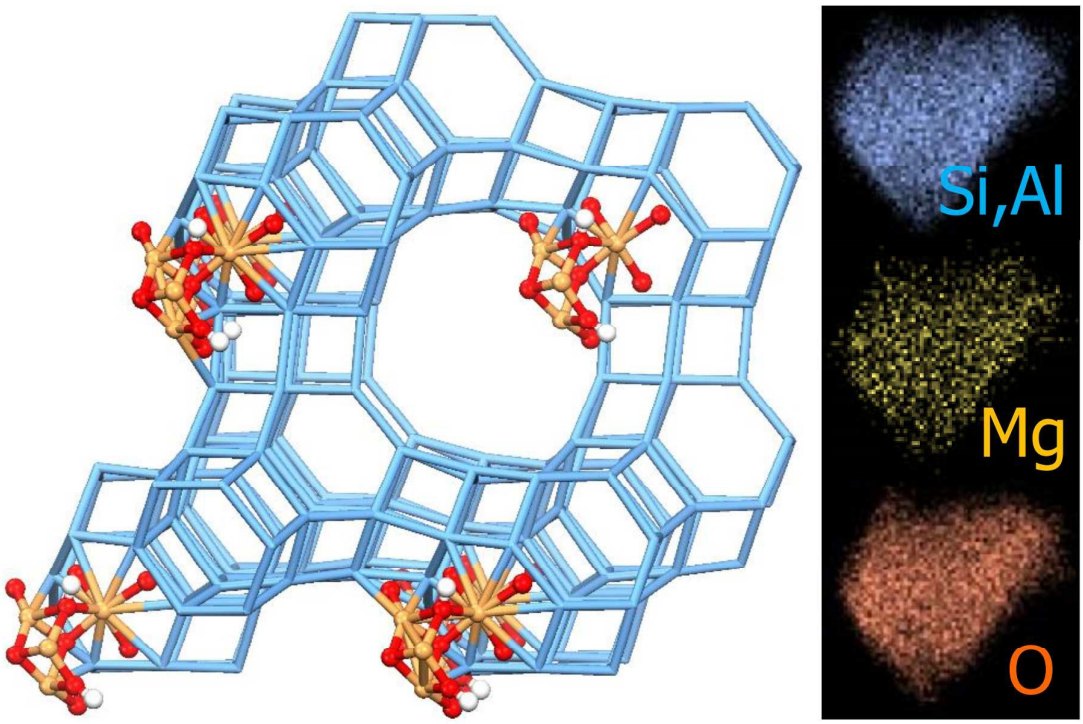

"Theory and experiment reveal the structure of magnesium oxide nanoclusters in a superbasic Faujasite zeolite."